Journal of Medicinal Chemistry

pubs.acs.org/jmc

Featured Article

Identification of MRTX1133, a Noncovalent, Potent, and Selective KRAS^{G12D} Inhibitor

Xiaolun Wang,* Shelley Allen, James F. Blake, Vickie Bowcut, David M. Briere, Andrew Calinisan, Joshua R. Dahlke, Jay B. Fell, John P. Fischer, Robin J. Gunn, Jill Hallin, Jade Laguer, J. David Lawson, James Medwid, Brad Newhouse, Phong Nguyen, Jacob M. O'Leary, Peter Olson, Spencer Pajk, Lisa Rahbaek, Mareli Rodriguez, Christopher R. Smith, Tony P. Tang, Nicole C. Thomas, Darin Vanderpool, Guy P. Vigers, James G. Christensen, and Matthew A. Marx*

Cite This: *J. Med. Chem.* 2022, 65, 3123−3133

Read Online

ACCESS | Metrics & More | Article Recommendations | Supporting Information

ABSTRACT: KRAS^{G12D}, the most common oncogenic KRAS mutation, is a promising target for the treatment of solid tumors. However, when compared to KRAS^{G12C}, selective inhibition of KRAS^{G12D} presents a significant challenge due to the requirement of inhibitors to bind KRAS^{G12D} with high enough affinity to obviate the need for covalent interactions with the mutant KRAS protein. Here, we report the discovery and characterization of the first noncovalent, potent, and selective KRAS^{G12D} inhibitor, MRTX1133, which was discovered through an extensive structure-based activity improvement and shown to be efficacious in a KRAS^{G12D} mutant xenograft mouse tumor model.

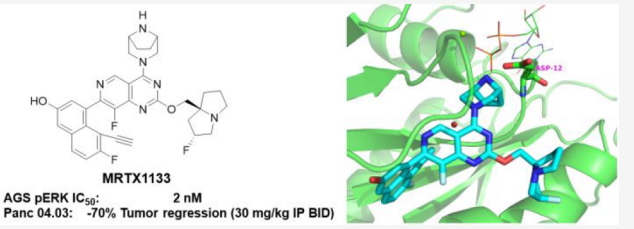

INTRODUCTION

Mutant KRAS has been recognized as an attractive drug target for the treatment of a number of cancers for many decades.[1−4] However, the high affinity of KRAS for GDP/GTP and the lack of any other apparent binding pocket have significantly hampered the development of KRAS inhibitors until recently.[1,4] The identification and subsequent clinical success of irreversible KRAS^{G12C} inhibitors that occupy the induced switch II pocket has been a very important breakthrough.[5−7] However, their inhibitory activity relies on a reactive warhead forming a stable covalent bond with the mutant Cys12. Conversely, KRAS^{G12D}, the most common mutation (33%) among KRAS mutant tumors,[8] lacks a reactive residue adjacent to the switch II pocket as evidenced in recent attempts,[9,10] and thus requires a novel approach toward the identification of selective inhibitors. A new class of KRAS inhibitors (for example, compound **2** in Figure 1) binding to a shallow pocket between switch I and II was reported[11−14] contemporaneously with the development of irreversible KRAS^{G12C} inhibitors; however, limited cellular activity was observed. Cyclic peptide KRAS^{G12D} inhibitors (for example, compound **3** in Figure 1) were also reported.[15−18] Although these peptides demonstrated better biochemical activity than the indole analogs illustrated by compound **2**, their physicochemical properties limited their cellular potency. Recently, a bicyclic peptidyl Pan-RAS inhibitor with submicromolar cellular potency and *in vivo* efficacy was reported.[19−21]

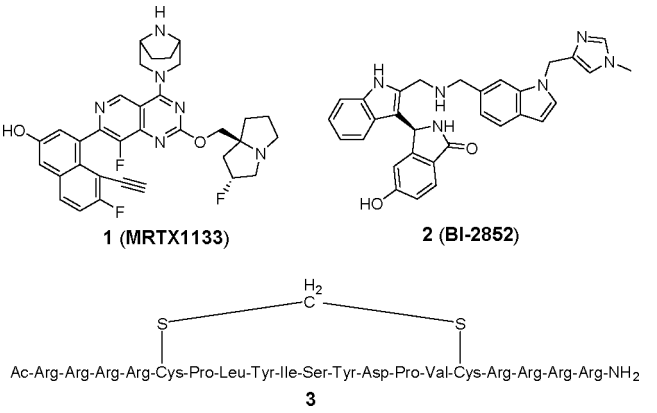

Figure 1. KRAS^{G12D} inhibitors.

We report herein the structure-based optimization of a series of molecules culminating in the discovery of **MRTX1133** (Figure 1, compound **1**), a potent, selective, noncovalent KRAS^{G12D} inhibitor with picomolar binding affinity, single digit nanomolar activity in cellular assays, and marked *in vivo*

Received: September 28, 2021
Published: December 10, 2021

efficacy in tumor models harboring $KRAS^{G12D}$ mutations. At the initiation of our $KRAS^{G12D}$-directed drug discovery activities, we were uncertain whether therapeutically meaningful $KRAS^{G12D}$ inhibition could be achieved with a noncovalent inhibitor, as the kinetic study for an early $KRAS^{G12C}$ irreversible inhibitor, ARS-853, revealed a modest K_I of 200 μM.[22] Later reports on ARS-1620, sotorasib, and adagrasib also demonstrated reversible affinities in the μM range.[5,23] Thus, we anticipated that significant improvements to binding affinity would be needed to achieve potency necessary for requisite target inhibition in cells. Therefore, we focused on maximizing the contribution of each moiety of the inhibitor to increase affinity, expecting that greater occupancy of the induced switch II pocket would lead to sustained functional suppression of KRAS pathway signaling in cellular and tumor environments harboring the $KRAS^{G12D}$ mutation sufficient for antitumor efficacy.

RESULTS AND DISCUSSION

Informed by our experience in discovering the $KRAS^{G12C}$ inhibitor adagrasib (compound **4**),[5,24] we synthesized compounds **5A** and **5B** with a pyrido[4,3-*d*]pyrimidine scaffold[25] with the anticipation that the protonated piperazine could interact productively with the mutant Asp12 side chain. Although compound **5A** was inactive, analog **5B** without the cyanomethyl group demonstrated a K_D of 3.5 μM in a $KRAS^{G12D}$ SPR assay with GDP-loaded $KRAS^{G12D}$ (Figure 2).

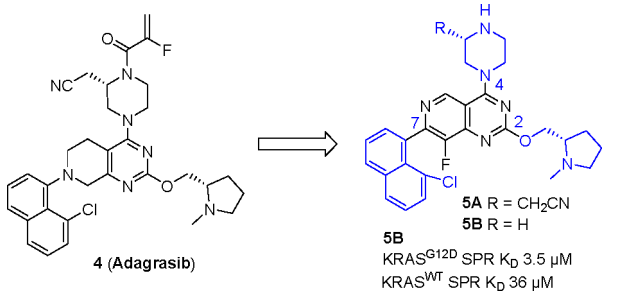

Figure 2. Pyrido[4,3-*d*]pyrimidine analog.

While the cyanomethyl group on the 3-position of the piperazine ring was found beneficial for irreversible $KRAS^{G12C}$ inhibitors[5] by displacing a water molecule close to Gly10 and enhancing the reactivity of the acrylamide warhead, compounds **5A** and **5B** suggested that a different approach would be needed to enhance $KRAS^{G12D}$ binding affinity in this region of the molecule for the pyrido[4,3-*d*]pyrimidine core. We also evaluated an analog of compound **5B** with the tetrahydropyridopyrimidine core[5,24,26,27] present in adagrasib, and found it to be 5−10-fold less potent than **5B**. Thus, the pyrido[4,3-*d*]pyrimidine scaffold was selected as a starting point for further optimization (Figure 2). The crystal structure of compound **5B** with $KRAS^{G12D}$/GDP (Figure 3) revealed that its placement in the switch II pocket resembled the binding mode of adagrasib with $KRAS^{G12C}$ (6UT0).[5] The hydrogen bond interaction of the 6-position nitrogen with Arg68 and the occupancy of the 8-fluorine in a small hydrophobic pocket may help explain why the pyrido[4,3-*d*]pyrimidine core is more potent than the corresponding tetrahydropyridopyrimidine. The three substituents of the pyrido[4,3-*d*]pyrimidine core interact extensively with the protein (Figure 3). The protonated piperazinyl group at the C4-position forms an

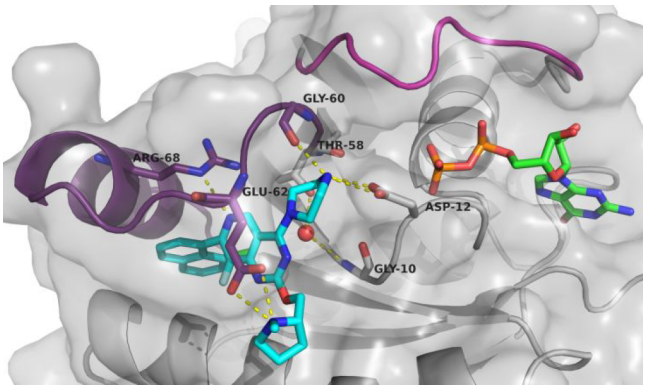

Figure 3. X-ray structure of compound **5B** with $KRAS^{G12D}$/GDP (7RT4).

ionic pair with the mutant Asp12, providing 10-fold selectivity over $KRAS^{WT}$. The piperazine twist-boat conformation (previously observed in the adagrasib/$KRAS^{G12C}$ structure[5]) and its salt bridge with Asp12 are stabilized by an additional hydrogen bond to the carbonyl oxygen of Gly60. The conserved water molecule under the C2-substituent forms hydrogen bonds with Gly10 and Thr58 but has no apparent interaction with compound **5B,** thus providing an opportunity for further exploration. The positively charged pyrrolidinyl moiety at the C2-position is well positioned for a favorable ionic interaction[28] with Glu62. Finally, the C7-naphthyl occupies a deep hydrophobic pocket as reported previously for adagrasib.[5,24] These three vectors were identified as opportunities to increase affinity for the $KRAS^{G12D}$ protein.

Given the importance of the salt bridge with Asp12 to the binding and selectivity of this lead molecule, we began optimization of the series at the C4-position using the C7-naphthol substituent (Table 1) identified in our earlier $KRAS^{G12C}$ effort.[24] The affinity of compound **6** with an unsubstituted piperazinyl group was 0.19 μM, while the homopiperazine analog **7** was 2-fold less potent. Both *N*-methylation (**8**) and the replacement of the secondary amino group with an oxygen (**9**) were deleterious. Moreover, compounds **8** and **9** lost selectivity over $KRAS^{WT}$ (SPR K_D = 6.2 and 0.56 μM, respectively). These observations further confirmed the importance of the ionized piperazine's bifurcated interactions with Asp12 and Gly60 for both activity and specificity. Methyl-substitution of the piperazine (**10** and **11**) did not improve potency. However, rigidification[29] of bioactive conformation[30,31] in piperazine analogs **12**−**15** increased affinity. Compound **15** with a [3.2.1]bicyclic diamino substituent had a K_D of 0.8 nM and possessed greater than 200-fold selectivity for $KRAS^{G12D}$ compared with $KRAS^{WT}$ (K_D = 182 nM). Consistent with the increased affinity, appreciable cell activity (pERK IC_{50} = 0.530 μM against AGS, a $KRAS^{G12D}$ cell line) was also observed for **15**. This provided early promise for the possibility of identifying an effective $KRAS^{G12D}$ inhibitor. The X-ray structure of compound **15** with $KRAS^{G12D}$/GDP is shown in Figure 4. The two-carbon bridge of the bicyclic group occupies a small pocket, while one of the endo C-Hs forms a nonclassical hydrogen bond with the Gly10 carbonyl oxygen.[32,33] It also positions the charged secondary amine for optimal interactions with Asp12 and Gly60. At this point, we developed an HTRF assay with GDP-loaded $KRAS^{G12D}$ using a probe based on compound **15** to increase screening throughput. The relative

https://doi.org/10.1021/acs.jmedchem.1c01688
J. Med. Chem. 2022, 65, 3123−3133

Table 1. Exploration of the C4-Position of Pyrido[4,3-*d*]pyrimidine[a]

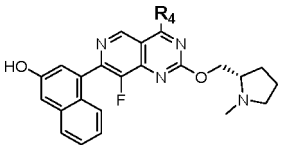

Comp.	R_4	SPR KRAS^{G12D} K_D (μM)	HTRF KRAS^{G12D} IC_{50} (μM)
6		0.19	0.98
7		0.42	2.6
8		8.7	54
9		1.5	12
10[&]		0.38	2.1
11[&]		0.28	1.5
12[&]		0.096	0.65
13[&]		0.009	0.068
14		0.073	0.31
15		0.0008	0.005

[a]& represents a diastereomeric mixture as the racemic amine was used for C4-substitution.

potency rankings of the HTRF assay aligned well with SPR affinity (Table 1), leading us to use the HTRF assay for subsequent compound profiling.

With a highly potent and selective C4 substitution in hand, we next focused on optimizing the C2 position of the core, which is summarized in Table 2. Deletion of the C2-pyrrolidinyl substitution in **15** yielded compound **16**, which resulted in an almost 600-fold decrease in potency, confirming the importance of this moiety for affinity. Compounds **17** and **18** were designed to interact with Glu62 in a similar fashion to **15**, but both only yielded a 42-fold increase in potency over **16**, likely due to lack of rigidity (**17**) and suboptimal interaction geometry (**18**). The activity of compound **19** with a basic imidazole group was comparable to that of **17** or **18** but was less potent than the pyrrolidinyl analog **15**. The focus of the C2-substituent design was then turned to

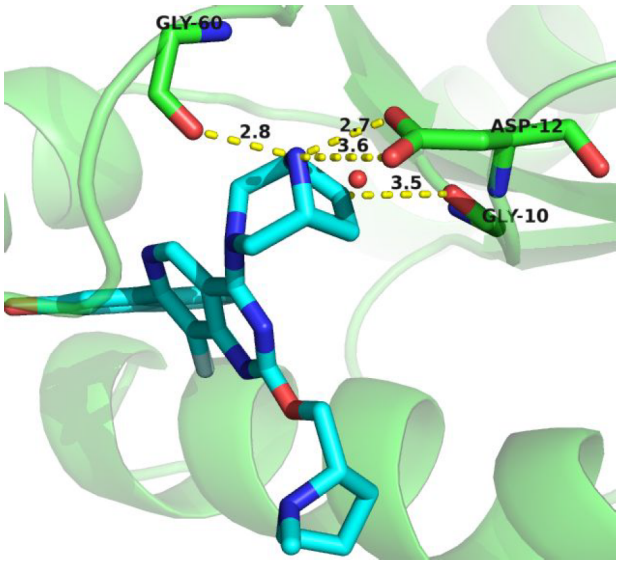

Figure 4. X-ray structure of compound **15** with KRAS^{G12D}/GDP (7RT1).

conformationally constrained amines. While the activity of the bridged morpholine **20** was inferior, the pyrrolizidine analog **21** provided over a 2-fold increase in cellular potency compared to **15**. Further optimization revealed the rigid 5,5-fused bicycle was preferred over the 6,5 system (**22**), and the basicity at this position is crucial for activity (**23**). Modification of the pyrrolizidine with a 2-fluoro substituent led to the discovery of the potent enantiomeric pair **24** and **25**. The IC_{50} of eutomer **25** in the pERK inhibition cell assay was 24 nM, 11-fold more active than the parent compound **21**. The absolute configuration of both enantiomers was confirmed by X-ray crystal structures with KRAS^{G12D}/GDP (Figure 5). As expected, the protonated pyrrolizidine forms a strong ionic interaction (N−O distances: 2.8 and 3.3 Å) with the negatively charged carboxylate of Glu62 (Figure 6). Interestingly, the 3-carbon of pyrrolizidine sits 3.4 Å from one of carboxylate oxygens suggesting a nonclassical hydrogen bond.[32,33] While the electron withdrawing nature of the fluorine atom likely reinforces both the ionic and nonclassical H-bond interactions in **25**, the shift of the fluorine position reduces the polarization of the C5 proton in **24** and may explain the slight activity difference between the two enantiomers.

The C7-substituent of the pyrido[4,3-*d*]pyrimidine is buried deeply in the binding site, and a small hydrophobic pocket near the 8-position of the naphthyl[5] provided an opportunity for further optimization. For this exploration, the readily prepared naphthyl derivatives, rather than the more elaborated naphthols, were utilized. Simple naphthyl 8-substituents such as methyl, fluorine, or chlorine provided an 8- to 30-fold activity boost (Table 3, compounds **27**, **28**, and **29**) over the unsubstituted **26** indicating that optimally filling this pocket may yield further improvement in activity. Furthermore, the substitutions also stabilized the preferred perpendicular conformation of the naphthyl ring. Extending the alkyl group from methyl to ethyl (**30**) provided another 7-fold increase in affinity, suggesting the terminal carbon favorably filled the hydrophobic space perpendicular to the 8-position of the naphthyl. However, a methoxy group at this position (**31**) was detrimental. Dihedral energy profiling (Figure 7) revealed that this was likely due to the terminal carbon preferring an

https://doi.org/10.1021/acs.jmedchem.1c01688
J. Med. Chem. 2022, 65, 3123−3133

Table 2. Examination of the 2-Substitution of Pyrido[4,3-*d*]pyrimidine[a]

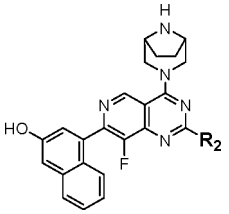

Comp.	R_2	HTRF KRAS^{G12D} IC_{50} (μM)	pERK AGS IC_{50} (μM)
15		0.005	0.53
16		2.96	>10
17	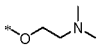	0.070	>10
18		0.069	1.3
19	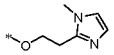	0.030	3.5
20	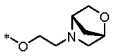	0.062	3.0
21		<0.002	0.27
22[&]		0.012	0.65
23[&]	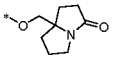	0.75	>10
24	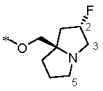	<0.002	0.064
25	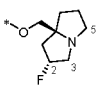	<0.002	0.024

[a]& represents racemic as the racemic amine was used for C4-substitution.

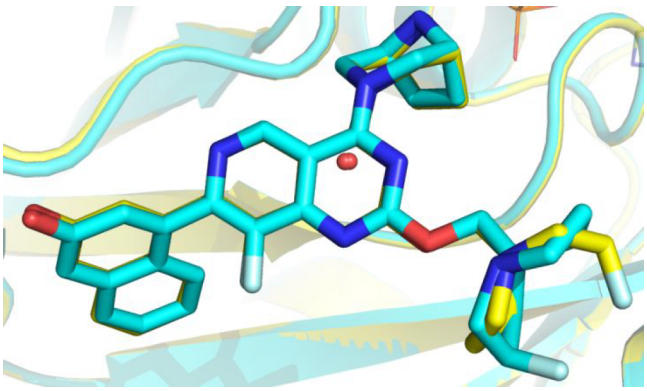

Figure 5. Overlay of the X-ray structures of compounds **24** (yellow, 7RT3) and **25** (cyan, 7RT2) with KRAS^{G12D}/GDP.

approximately coplanar orientation to the naphthyl group, while the preferred conformation of the ethyl group of 108° is

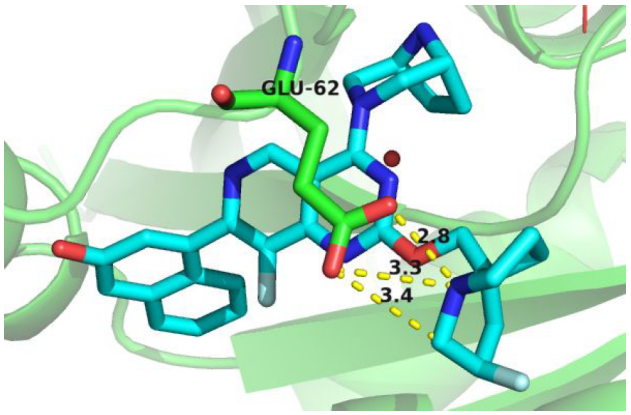

Figure 6. Interaction of 2-Fluoropyrrolizidine (**25**) with Glu62.

close to the modeled binding pose of 100°. The energy calculations predicted a 15-fold difference in binding affinity, consistent with the observed potency shift between **30** and **31**. It has been recognized in our previously reported KRAS^{G12C} structures that a conserved water molecule makes hydrogen bond interactions with both Gly10 and Thr58,[5] and we envisioned that a hydrogen bond donor (HBD) from the 8-position of the naphthyl group might further stabilize this hydrogen bond network. The initial attempt with the introduction of a hydroxyl group (**32**) was unsuccessful. A careful examination suggested an 8-ethynyl substitution would not only fill the hydrophobic space well, but could also engage the conserved water molecule via a nonclassical HBD.[34,35] Indeed, the 8-ethynyl analog **33** was 120-fold more potent than the parent compound **26**. Next, we turned our attention to a small pocket near to the side chains of Val9, Phe78, and Ile100. A fluorine atom at the 7-position of the naphthyl (**34**) was introduced to fill this space and provided a 13-fold increase in potency over unsubstituted **26**. This effect was additive with the activity increases observed when combined with selected substituents at the 8-position as evidenced in the pairs of **27** vs **35** and **33** vs **36**. The biochemical activity of compound **36** with the optimized 7-fluoro-8-ethynylnaphthyl was less than 2 nM and its IC_{50} in the cellular pERK assay was 24 nM, the most potent compound identified of the des-naphthol analogs. However, compound **36** demonstrated limited pERK inhibition in KRAS^{G12D} mutated tumor xenografts when intraperitoneally administered *in vivo* at the maximal tolerated dose (30 mg/kg, AUC_{0-24} = 9495 ng·h/mL) indicating further improvement of potency and/or physiochemical properties was needed for suitable levels of target inhibition. The X-ray structure of **36** in KRAS^{G12D}/GDP revealed that the 7-fluoro and 8-ethynyl substituents are nicely positioned in a hydrophobic pocket formed with Val9, Thr58, Phe78, Met72, Tyr96, and Ile100 (Figure 8). The conserved water molecule is hydrogen-bonded to two HBAs, the hydroxyl from Thr58 and the carbonyl oxygen from Gly10, and two HBDs, the alkynyl proton of the ligand and NH of Gly10, forming a well-organized hydrogen bond network (Figure 9a,b). These interactions allow the terminal alkynyl group to effectively bridge the lipophilic and polar regions of the switch II pocket. Reintroduction of the naphthol (**37**, **38**) confirmed that the potency increases derived from 3- and 8-naphthyl substitutions are indeed combinable.

Finally, the combination of the optimized three substituents on the 2-, 4-, and 7-positions of pyrido[4,3-*d*]pyrimidine led to

https://doi.org/10.1021/acs.jmedchem.1c01688
J. Med. Chem. 2022, 65, 3123−3133

Table 3. Evaluation of the C7-Position of Pyrido[4,3-*d*]pyrimidine

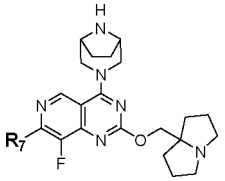

Comp.	R_7	HTRF KRAS^{G12D} IC_{50} (μM)	pERK AGS IC_{50} (μM)
26		0.36	>10
27		0.012	0.38
28		0.015	0.19
29		0.045	2.5
30		0.006	0.20
31		0.086	1.2
32	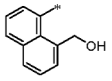	0.079	>10
33		0.003	0.071
34		0.027	0.37
35		0.007	0.097
36		<0.002	0.024
37	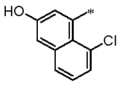	<0.002	0.063
38	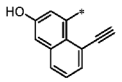	<0.002	0.014

the discovery of MRTX1133, an exceptionally potent and selective KRAS^{G12D} inhibitor (Figure 10). MRTX1133 optimally fills the switch II pocket and extends three substituents to favorably interact with the protein (Figure 11), resulting in an estimated K_D against KRAS^{G12D} of 0.2 pM. AlphaLISA data confirmed that binding of the inhibitor prevented SOS1-catalyzed nucleotide exchange and/or formation of the KRAS^{G12D}/GTP/RAF1 complex, thereby inhibiting mutant KRAS-dependent signal transduction.

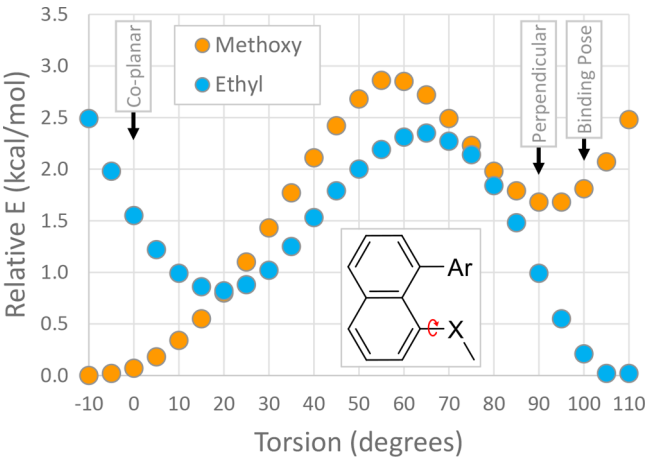

Figure 7. Preferred conformation of 8-substitutions in **30** and **31**. Dihedral scan performed for 8-substituted ethyl (blue) and methoxy (orange) analogs in Spartan[36] using ωB97X-D/6-31G**. Ar represents the 8-fluoro-azaquinazoline ring which was held in the binding nascent pose during the scan

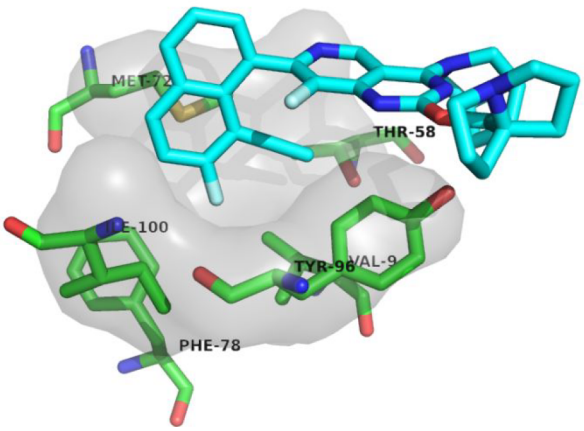

Figure 8. Residues around 7-fluoro-8-ethynylnaphthyl in the X-ray structure of compound **36** with KRAS^{G12D}/GDP.

MRTX1133 inhibited ERK phosphorylation in the AGS cell line with an IC_{50} of 2 nM (see Table S2 for activity against a panel of KRAS^{G12D} cell lines). In a 2D viability assay, the IC_{50} of MRTX1133 was 6 nM against the same cell line, while demonstrating more than 500-fold selectivity against MKN1, a cell line which is dependent on KRAS for its growth and survival due to the amplification of wild-type *KRAS*[37] (Table 4).

Intraperitoneal (IP) administration of MRTX1133 at 30 mg/kg in CD-1 mice (Figure 12) resulted in sustained plasma exposure exceeding the free-fraction-adjusted pERK IC_{50} value in the KRAS^{G12D} mutant Panc 04.03 cell line for approximately 8 h. Encouraged by this result, we evaluated the ability to modulate KRAS-dependent ERK phosphorylation in the Panc 04.03 xenograft tumor model at 30 mg/kg BID (IP) and observed 62% and 74% inhibition of pERK signal at 1 and 12 h after the second dose, respectively (Figure 13). An antitumor efficacy study in this model resulted in MRTX1133 dose-dependent antitumor activity with 94% growth inhibition observed at 3 mg/kg BID (IP) and tumor regressions of −62% and −73% observed at 10 and 30 mg/kg BID (IP), respectively (Figure 14). In contrast, no significant antitumor activity was

https://doi.org/10.1021/acs.jmedchem.1c01688
J. Med. Chem. 2022, 65, 3123−3133

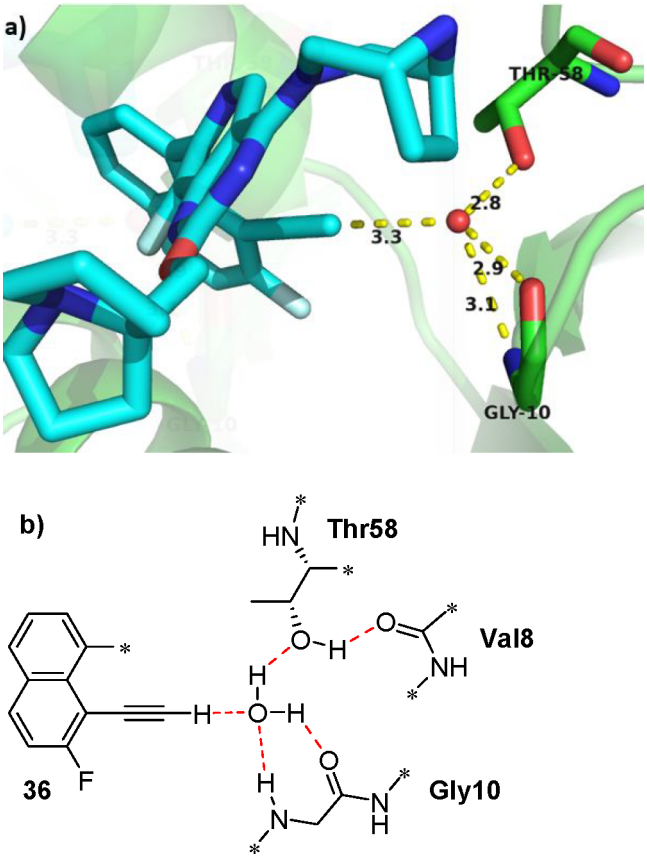

Figure 9. (a,b) Hydrogen network around the conserved water molecule in the X-ray structure of compound **36** with KRAS^{G12D}/GDP (7RT5).

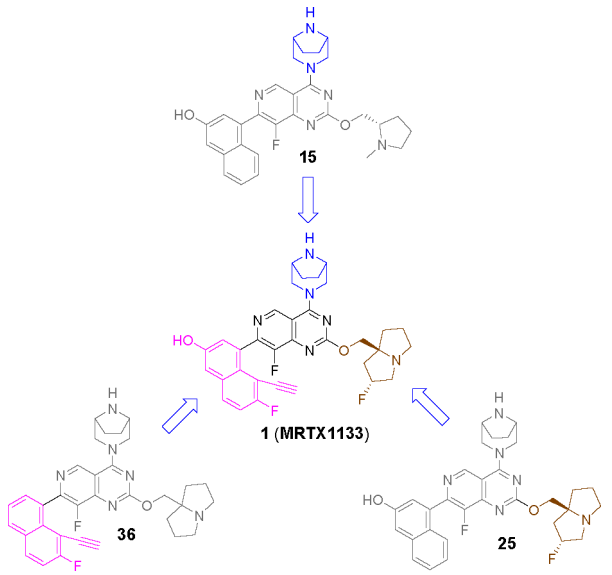

Figure 10. Design of MRTX1133.

observed in the non-KRAS^{G12D} tumor model MKN1 (data not shown).

Chemistry. The synthesis of compound **1** (Scheme 1) commenced with the chlorination of 7-chloro-8-fluoropyrido-[4,3-*d*]pyrimidine-2,4(1*H*,3*H*)-dione[25] **39** through the treatment of $POCl_3$ to afford 2,4,7-trichloro-8-fluoropyrido[4,3-*d*]pyrimidine **40**. The C4 substituent was introduced by a selective S_NAr with *tert*-butyl 3,8-diazabicyclo[3.2.1]octane-8-carboxylate followed by a second S_NAr with ((2*R*,7a*S*)-2-fluorotetrahydro-1*H*-pyrrolizin-7a(5*H*)-yl)methanol[25] to in-

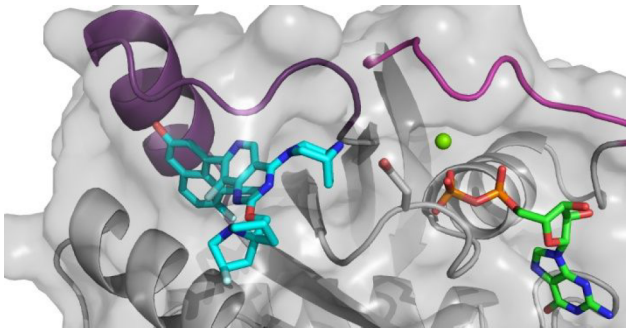

Figure 11. MRTX1133 with KRAS^{G12D}/GDP (7RPZ).

Table 4. *In Vitro* Profile of MRTX1133

assay	activity
KRAS^{G12D} K_D (nM)	~0.0002[a]
AlphaLISA IC_{50} (nM)	5
pERK AGS IC_{50} (nM)	2
2D viability AGS (KRAS^{G12D}) IC_{50} (nM)	6
2D viability MKN1 (KRAS^{WT}) IC_{50} (nM)	>3000

[a]The K_D value generated is beyond what the instrument can accurately determine but is reported as an approximate value.

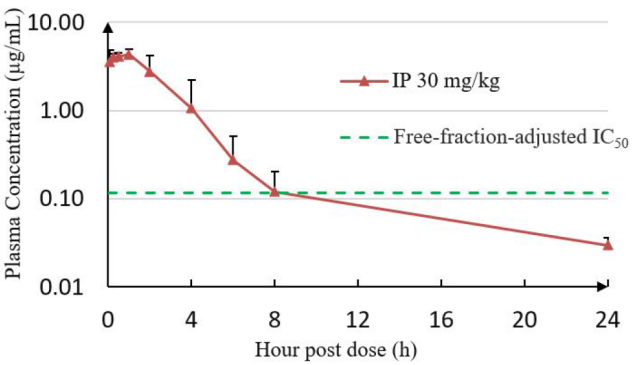

Figure 12. PK Curve of MRTX1133 in CD-1 mouse.

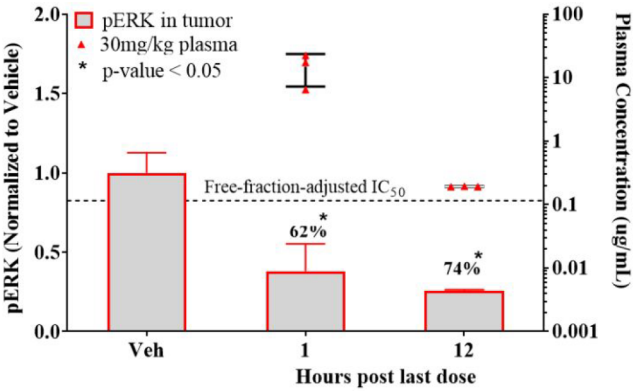

Figure 13. pERK modulation in Panc 04.03 model after intraperitoneal administration of MRTX1133. *p-value with t test assuming equal variance <0.05. Statistical analysis of differences in mean pERK inhibition between vehicle and MRTX1133-treated cohorts was run using a two-tailed Student's t test with equal variance in Excel (Microsoft; Redmond, WA).

https://doi.org/10.1021/acs.jmedchem.1c01688
J. Med. Chem. 2022, 65, 3123−3133

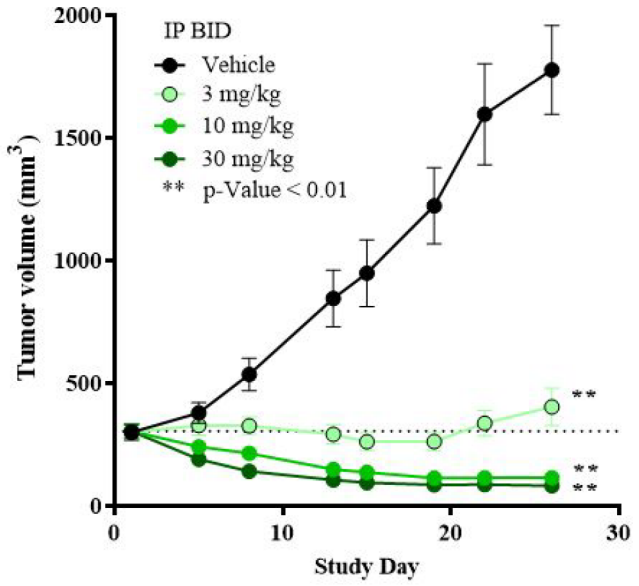

Figure 14. Efficacy of MRTX1133 in Panc 04.03 model. **p-value with t test assuming equal variance <0.01. Statistical analysis of differences in mean tumor volume between vehicle and MRTX1133-treated cohorts was run using a two-tailed Student's t test with equal variance in Excel (Microsoft; Redmond, WA).

Scheme 1. Synthesis of Compound 1[a]

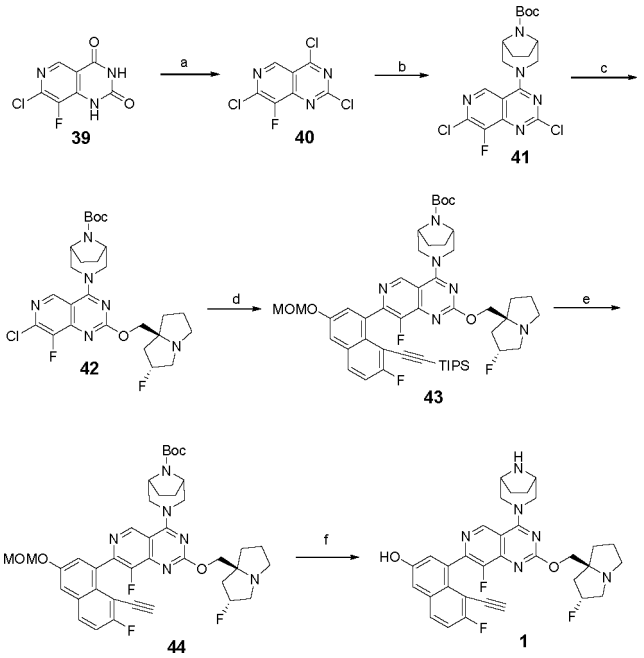

[a]Reagents and conditions. (a) $POCl_3$, *N*-ethyl-*N*-isopropylpropan-2-amine, 100 °C, 1 h; (b) *tert*-butyl 3,8-diazabicyclo[3.2.1]octane-8-carboxylate, *N*-ethyl-*N*-isopropylpropan-2-amine, CH_2Cl_2, −40 °C, 0.5 h, 42% (two steps); (c) ((2*R*,7a*S*)-2-fluorotetrahydro-1*H*-pyrrolizin-7a(5*H*)-yl)methanol, *N*-ethyl-*N*-isopropylpropan-2-amine, dioxane, 95 °C, 41 h, 55%; (d) ((2-fluoro-6-(methoxymethoxy)-8-(4,4,5,5-tetramethyl-1,3,2-dioxaborolan-2-yl)naphthalen-1-yl)-ethynyl)triisopropylsilane, Ad_2nBuP-Pd-G3, K_3PO_4, THF, 60 °C, 3 h, 76%; (e) HCl in dioxane, 0 °C, 1 h, 56%; (f) CsF, DMF, 20 °C, 1 h, 56%.

stall C2 moiety. Suzuki coupling of **42** with ((2-fluoro-6-(methoxymethoxy)-8-(4,4,5,5-tetramethyl-1,3,2-dioxaborolan-2-yl)naphthalen-1-yl)ethynyl)triisopropylsilane[38] provided intermediate **43**. The subsequent deprotections of the triisopropylsilyl and methoxymethyl ether groups resulted in the desired product **1**.

CONCLUSION

Through extensive structure-based drug design, MRTX1133 was identified as a noncovalent, potent, and selective inhibitor of $KRAS^{G12D}$. MRTX1133 suppresses $KRAS^{G12D}$ signaling in cells and *in vivo*, and its antitumor benefit was demonstrated in a murine animal model. To the best of our knowledge, this is the first report in the literature of a small molecule inhibitor of $KRAS^{G12D}$ that exhibits robust *in vivo* efficacy. These data support the potential for the advancement of an effective therapeutic against this "undruggable" target. The optimization process was facilitated by high-resolution X-ray crystal structures. In-depth binding mode analysis derived from cocrystal structures allowed the optimization of lipophilic contact of the inhibitor in the binding pocket and the identification of nonclassical hydrogen bonding and ion pair interactions, ultimately increasing selective binding affinity for $KRAS^{G12D}$ by more than 1,000,000-fold relative to the initial hit **5B**. MRTX1133 binds to the switch II pocket and inhibits the protein−protein interactions necessary for activation of the KRAS pathway. MRTX1133 not only possesses single-digit nM potency in a cellular proliferation assay, but also demonstrates tumor regressions in the Panc 04.03 xenograft model. A more comprehensive *in vitro* and *in vivo* pharmacological characterization of MRTX1133 will be disclosed in due course.

EXPERIMENTAL SECTION

All chemicals were purchased from commercial suppliers and used as received unless otherwise indicated. Proton nuclear magnetic resonance (^{1}H NMR) spectra were recorded on Bruker Avance 400 MHz spectrometers. Chemical shifts are expressed in δ ppm and are calibrated to the residual solvent peak: proton (e.g., $CDCl_3$, 7.27 ppm). Coupling constants (J), when given, are reported in hertz. Multiplicities are reported using the following abbreviations: s = singlet, d = doublet, dd = doublet of doublets, t = triplet, q = quartet, m = multiplet (range of multiplet is given), br = broad signal, dt = doublet of triplets. Carbon nuclear magnetic resonance (^{13}C NMR) spectra were recorded using a Bruker Avance HD spectrometer at 100 MHz. Chemical shifts are reported in parts per million (ppm) and are calibrated to the solvent peak: carbon ($CDCl_3$, 77.23 ppm). All final compounds were purified by reverse-phase high-performance liquid chromatography (HPLC) or supercritical fluid chromatography (SFC). The purity for test compounds was determined by high-performance liquid chromatography (HPLC) on a LC-20AB Shimadzu instrument. HPLC conditions were as follows: Kinetex C18 4.6 × 50 mm, 5 μm, 10−80% ACN (0.0375% TFA) in water (0.01875% TFA), 4 min run, flow rate 1.5 mL/min, UV detection (λ = 220, 215, 254 nm) or XBridge C18, 2.1 × 50 mm, 5 μm, 10−80% ACN in water buffered with 0.025% ammonia, 4 min run, flow rate 0.8 mL/min, UV detection (λ = 220, 215, 254 nm). The mass spectra were obtained using liquid chromatography mass spectrometry (LC-MS) on a LCMS-2020 Shimadzu instrument using electrospray ionization (ESI in the positive mode). LCMS conditions were as follows: Kinetex EVO C18 30 × 2.1 mm, 5 μm, 5−95% ACN (0.0375% TFA) in water (0.01875% TFA), 1.5 min run, flow rate 1.5 mL/min, UV detection (λ = 220, 254 nm), or Kinetex EVO C18 2.1 × 30 mm, 5 μm, 5−95% ACN in water buffered with 0.025% ammonia, 1.5 min run, flow rate 1.5 mL/min, UV detection (λ = 220, 254 nm). High resolution mass measurements were carried out on an Agilent 1290LC and 6530Q-TOF series with ESI. Optical rotation data were recorded on an Anton Paar MCP500 [length = 1 dm, sodium lamp, λ (nm) = 589, temperature = 25 °C]. The SFC purity

https://doi.org/10.1021/acs.jmedchem.1c01688
J. Med. Chem. 2022, 65, 3123−3133

for test compounds was determined with a Shimadzu LC-30ADsf. All compounds are >95% pure by HPLC.

Preparation of Compound 1 (MRTX1133).[38] *2,4,7-Trichloro-8-fluoropyrido[4,3-d]pyrimidine (**40**).* A mixture of 7-chloro-8-fluoropyrido[4,3-*d*]pyrimidine-2,4(1*H*,3*H*)-dione (5 g, 23 mmol, 1.0 equiv) and *N*-ethyl-*N*-isopropylpropan-2-amine (20 mL, 115 mmol, 5.0 equiv) in $POCl_3$ (50 mL, 535 mmol, 23 equiv) was stirred at 100 °C for 1 h. Then, the mixture was concentrated under vacuum to give crude title compound (6.5 g) as yellow oil, which was used in the next step without further purification.

*tert-Butyl (1R,5S)-3-(2,7-dichloro-8-fluoropyrido[4,3-d]-pyrimidin-4-yl)-3,8-diazabicyclo[3.2.1]octane-8-carboxylate (**41**).* To a solution of 2,4,7-trichloro-8-fluoropyrido[4,3-*d*]pyrimidine (6.5 g, crude) and *N*-ethyl-*N*-isopropylpropan-2-amine (26.9 mL, 154 mmol) in dichloromethane (20 mL) was added *tert*-butyl 3,8-diazabicyclo[3.2.1]octane-8-carboxylate (4.9 g, 23 mmol) at −40 °C. The reaction was stirred at −40 °C for 0.5 h. Then, 20 mL water was added to the reaction, and the mixture was extracted with dichloromethane (2 × 20 mL). The combined organic layers were washed with brine (30 mL), dried over Na_2SO_4, filtered, and concentrated under vacuum to afford the title compound as yellow solid (4 g, two steps 41% yield). LCMS [ESI, M+1]: 428.

*(1R,5S)-tert-Butyl 3-(7-chloro-8-fluoro-2-(((2R,7aS)-2-fluorohexahydro-1H-pyrrolizin-7a-yl)methoxy)pyrido[4,3-d]pyrimidin-4-yl)-3,8-diazabicyclo[3.2.1]octane-8-carboxylate (**42**).* To a solution of (1*R*,5*S*)-*tert*-butyl 3-(2,7-dichloro-8-fluoropyrido[4,3-*d*]pyrimidin-4-yl)-3,8-diazabicyclo[3.2.1]octane-8-carboxylate (53.8 g, 126 mmol, 1 equiv), ((2*R*,7a*S*)-2-fluorohexahydro-1*H*-pyrrolizin-7a-yl)methanol (20 g, 126 mmol, 1 equiv), and *N*-ethyl-*N*-isopropylpropan-2-amine (40.6 g, 314 mmol, 2.5 equiv) in dioxane (160 mL) was added 4 Å molecular sieve (20 g) at 20 °C. The suspension was stirred at 95 °C under N_2 for 41 h. The reaction was cooled to 60 °C and filtered. The filter cake was washed with ethyl acetate (0.1 L × 2) and dichloromethane (0.1 L). The filtrate was concentrated under reduced pressure to give a residue. The residue was dispersed in DMF (0.12 L), and the mixture was stirred at 60 °C for 1.5 h. The mixture was filtered, and the filter cake was washed with petroleum ether (0.1 L × 3) to give a solid. The solid was dried under reduced pressure to afford the title compound (43.6 g, 88% purity, 55% yield) as white solid; LCMS [ESI, M+1]: 551.2; ^{1}H NMR (400 MHz, $CDCl_3$) δ 8.72 (s, 1H), 5.28 (d, J = 54.4 Hz, 1H), 4.56−4.43 (m, 2H), 4.42−4.30 (m, 2H), 4.28−4.22 (m, 1H), 4.18−4.10 (m, 1H), 3.77−3.56 (m, 3H), 3.32−3.08 (m, 3H), 3.02−2.93 (m, 1H), 2.34−2.09 (m, 3H), 2.01−1.90 (m, 4H), 1.69 (d, J = 7.8 Hz, 2H), 1.52 (s, 9H).

*(1R,5S)-tert-Butyl-3-(8-fluoro-7-(7-fluoro-3-(methoxymethoxy)-8-((triisopropylsilyl)ethynyl)naphthalen-1-yl)-2-(((2R,7aS)-2-fluorohexahydro-1H-pyrrolizin-7a-yl)methoxy)pyrido[4,3-d]pyrimidin-4-yl)-3,8-diazabicyclo[3.2.1]octane-8-carboxylate (**43**).* To a mixture of (1*R*,5*S*)-*tert*-butyl 3-(7-chloro-8-fluoro-2-(((2*R*,7a*S*)-2-fluorohexahydro-1*H*-pyrrolizin-7*a*-yl)methoxy)pyrido[4,3-*d*]pyrimidin-4-yl)-3,8-diazabicyclo[3.2.1]octane-8-carboxylate (55 g, 87.8 mmol, 88% purity, 1.0 equiv) and K_3PO_4 (1.5 M, 176 mL, 3.0 equiv) in THF (275 mL) were added $Ad_2{}^nBuP$-Pd-G3 (6.4 g, 8.78 mmol, 0.1 equiv), and ((2-fluoro-6-(methoxymethoxy)-8-(4,4,5,5-tetramethyl-1,3,2-dioxaborolan-2-yl)naphthalen-1-yl)ethynyl)triisopropylsilane (49.5 g, 96.6 mmol, 1.1 equiv) in one portion under N_2.The mixture was stirred at 60 °C for 3 h. After completion, the mixture was concentrated under reduced pressure to give a residue. The residue was purified with column chromatography (Al_2O_3, petroleum ether/ethyl acetate = 20/1 to 5/1) to give a crude product. Then, it was purified by reversed-phase HPLC (C18, 0.1% FA in water, 0−100% MeCN) to afford the title compound (63.3 g, 95% purity, 76% yield) as yellow solid; LCMS [ESI, M+1]: 901.4; ^{1}H NMR (400 MHz, methanol-d_4) δ 8.99 (d, J = 2.1 Hz, 1H), 7.87 (dd, J = 5.7, 9.1 Hz, 1H), 7.56 (d, J = 2.6 Hz, 1H), 7.30 (t, J = 8.9 Hz, 1H), 7.22 (t, J = 2.3 Hz, 1H), 5.29−5.10 (m, 3H), 4.82 (br t, J = 11.2 Hz, 1H), 4.38−4.06 (m, 5H), 3.79 (br dd, J = 6.1, 11.9 Hz, 1H), 3.43−3.35 (m, 4H), 3.18−3.05 (m, 3H), 2.91 (dt, J = 5.6, 9.5 Hz, 1H), 2.23−2.00 (m, 3H), 1.91−1.56 (m, 7H), 1.43 (s, 9H), 0.85−0.74 (m, 18H), 0.44 (q, J = 7.5 Hz, 3H).

(1R,5S)-tert-Butyl-3-(7-(8-ethynyl-7-fluoro-3-(methoxymethoxy)-naphthalen-1-yl)-8-fluoro-2-(((2R,7aS)-2-fluorohexahydro-1H-pyrrolizin-7a-yl)methoxy)pyrido[4,3-d]pyrimidin-4-yl)-3,8-diazabicyclo[3.2.1]octane-8-carboxylate. To a solution of (1*R*,5*S*)-*tert*-butyl 3-(8-fluoro-7-(7-fluoro-3-(methoxymethoxy)-8-((triisopropylsilyl)ethynyl)naphthalen-1-yl)-2-(((2*R*,7a*S*)-2-fluorohexahydro-1*H*-pyrrolizin-7*a*-yl)methoxy)pyrido[4,3-*d*]pyrimidin-4-yl)-3,8-diazabicyclo[3.2.1]octane-8-carboxylate (42.0 g, 46.6 mmol, 1.0 equiv) in DMF (160 mL) was added CsF (70.8 g, 466 mmol, 17.2 mL, 10 equiv) in one portion under N_2. The mixture was stirred at 20 °C for 1 h. After completion, the mixture was purified with reversed-phase HPLC (C18, 0.1% FA in water, 0−100% MeCN) to afford the title compound (30.3 g, 87% yield) as yellow solid (**44**); LCMS [ESI, M+1]: 745.2.

*4-(4-((1R,5S)-3,8-Diazabicyclo[3.2.1]octan-3-yl)-8-fluoro-2-(((2R,7aS)-2-fluorohexahydro-1H-pyrrolizin-7a-yl)methoxy)pyrido-[4,3-d]pyrimidin-7-yl)-5-ethynyl-6-fluoronaphthalen-2-ol (**1**).* To a mixture of (1*R*,5*S*)-*tert*-butyl 3-(7-(8-ethynyl-7-fluoro-3-(methoxymethoxy)naphthalen-1-yl)-8-fluoro-2-(((2*R*,7a*S*)-2-fluorohexahydro-1*H*-pyrrolizin-7a-yl)methoxy)pyrido[4,3-*d*]pyrimidin-4-yl)-3,8-diazabicyclo[3.2.1]octane-8-carboxylate (40.0 g, 53.7 mmol, 1.0 equiv) and MeCN (240 mL) was added HCl/dioxane (4 M, 240 mL, 17.9 equiv) in one portion at 0 °C under N_2. The mixture was stirred at 0 °C for 1 h. After completion, the mixture was concentrated under reduced pressure to give a residue, and the residue was basified with $NaHCO_3$ solution (pH = 8). The mixture was extracted with MeOH and DCM twice. The combined organic phases were dried with anhydrous Na_2SO_4, filtered, and concentrated in vacuum to give the crude product. Then it was purified with reverse-phase HPLC (C18, 0.1% FA in water, 0−100% MeCN). The desired fractions were combined, basified with $NaHCO_3$ (pH = 8), and extracted with MeOH and DCM twice. The combined organic phases were dried with anhydrous Na_2SO_4, filtered, and concentrated in vacuum to give a residue. The residue was then purified with another reverse-phase HPLC [column: Phenomenex luna C18 250 mm × 100 mm × 10 μm, mobile phase: A: water (0.1% TFA), B: ACN, B %: 12−38% 23 min]. The desired fractions were combined, basified with $NaHCO_3$ (pH = 8), and extracted with MeOH and DCM twice. The combined organic phases were dried with anhydrous Na_2SO_4, filtered, and concentrated in vacuum to give a residue. The residue was then lyophilized to afford the title compound (18.2 g, 56% yield, 99.7% purity) as yellow solid; LCMS [ESI, M+1]: 601.3; SFC: >99% ee, Chiralpak IC-3 50 × 4.6 mm I.D., 3 μm column A: CO_2, B: MeOH (0.05% DEA), 3 mL/min, 220 nm, t_R: 1.762 min; $[\alpha]_D$ (25 °C): + 10.143° (c = 0.38 g/100 mL, MeOH); ^{1}H NMR (400 MHz, methanol-d_4) δ 9.02 (s, 1H), 7.87 (dd, J = 5.8, 9.1 Hz, 1H), 7.39−7.30 (m, 2H), 7.23 (d, J = 2.5 Hz, 1H), 5.42−5.23 (m, 1H), 4.70−4.55 (m, 2H), 4.3−4.20 (m, 2H), 3.80−3.62 (m, 4H), 3.36 (dd, J = 0.9, 6.9 Hz, 1H), 3.32−3.14 (m, 3H), 3.03 (dt, J = 5.7, 9.5 Hz, 1H), 2.41−2.11 (m, 3H), 2.07−1.97 (m, 2H), 1.96−1.75 (m, 5H); ^{13}C NMR (100 MHz, methanol-d_4) δ 166.42, 165.78, 165.58, 163.11, 155.84, 155.82, 153.92, 151.37, 150.58, 150.46, 146.94, 146.79, 145.23, 145.17, 134.80, 134.39, 131.70, 131.61, 127.26, 124.36, 117.29, 117.03, 113.25, 112.44, 105.68, 105.52, 99.91, 98.17, 90.13, 90.09, 90.07, 76.36, 74.93, 74.36, 61.60, 61.41, 58.40, 56.47, 56.40, 56.32, 56.28, 55.78, 55.75, 43.82, 43.62, 37.35, 28.74, 28.66, 26.45. HRMS(ESI+) calcd for $C_{33}H_{32}F_3N_6O_2^+$ ($M+H^+$) 601.2533, found 601.2533.

■ ASSOCIATED CONTENT

Supporting Information

The Supporting Information is available free of charge at https://pubs.acs.org/doi/10.1021/acs.jmedchem.1c01688.

Synthetic experimental procedures for compound **5** to **38**; NMR spectra and HPLC trace of final Compounds; HTRF, SPR, AlphaLISA, and cellular assay protocols; *in vivo* PK/PD and TGI studies (PDF)

https://doi.org/10.1021/acs.jmedchem.1c01688
J. Med. Chem. 2022, 65, 3123−3133

Molecular formula strings (CSV)

Accession Codes

PDB code: 7RPZ, 7RT1, 7RT2, 7RT3, 7RT4, 7RT5.

AUTHOR INFORMATION

Corresponding Authors

Xiaolun Wang − *Mirati Therapeutics, San Diego, California 92121, United States*; orcid.org/0000-0001-9576-7746; Phone: 858-401-6730; Email: wangx@mirati.com

Matthew A. Marx − *Mirati Therapeutics, San Diego, California 92121, United States*; Phone: 858-332-3558; Email: marxm@mirati.com

Authors

Shelley Allen − *Pfizer Boulder Research & Development, Boulder, Colorado 80301, United States*

James F. Blake − *Pfizer Boulder Research & Development, Boulder, Colorado 80301, United States*

Vickie Bowcut − *Mirati Therapeutics, San Diego, California 92121, United States*

David M. Briere − *Mirati Therapeutics, San Diego, California 92121, United States*

Andrew Calinisan − *Mirati Therapeutics, San Diego, California 92121, United States*

Joshua R. Dahlke − *Pfizer Boulder Research & Development, Boulder, Colorado 80301, United States*

Jay B. Fell − *Pfizer Boulder Research & Development, Boulder, Colorado 80301, United States*

John P. Fischer − *Pfizer Boulder Research & Development, Boulder, Colorado 80301, United States*

Robin J. Gunn − *Mirati Therapeutics, San Diego, California 92121, United States*

Jill Hallin − *Mirati Therapeutics, San Diego, California 92121, United States*

Jade Laguer − *Mirati Therapeutics, San Diego, California 92121, United States*

J. David Lawson − *Mirati Therapeutics, San Diego, California 92121, United States*

James Medwid − *Mirati Therapeutics, San Diego, California 92121, United States*

Brad Newhouse − *Pfizer Boulder Research & Development, Boulder, Colorado 80301, United States*

Phong Nguyen − *Pfizer Boulder Research & Development, Boulder, Colorado 80301, United States*

Jacob M. O'Leary − *Pfizer Boulder Research & Development, Boulder, Colorado 80301, United States*

Peter Olson − *Mirati Therapeutics, San Diego, California 92121, United States*

Spencer Pajk − *Pfizer Boulder Research & Development, Boulder, Colorado 80301, United States*

Lisa Rahbaek − *Mirati Therapeutics, San Diego, California 92121, United States*

Mareli Rodriguez − *Pfizer Boulder Research & Development, Boulder, Colorado 80301, United States*

Christopher R. Smith − *Mirati Therapeutics, San Diego, California 92121, United States*

Tony P. Tang − *Pfizer Boulder Research & Development, Boulder, Colorado 80301, United States*

Nicole C. Thomas − *Mirati Therapeutics, San Diego, California 92121, United States*

Darin Vanderpool − *Mirati Therapeutics, San Diego, California 92121, United States*

Guy P. Vigers − *Pfizer Boulder Research & Development, Boulder, Colorado 80301, United States*

James G. Christensen − *Mirati Therapeutics, San Diego, California 92121, United States*

Complete contact information is available at: https://pubs.acs.org/10.1021/acs.jmedchem.1c01688

Author Contributions

The manuscript was written through contributions of all authors. All authors have given approval to the final version of the manuscript.

Notes

Authors will release the atomic coordinates and experimental data upon article publication.

The authors declare no competing financial interest.

ACKNOWLEDGMENTS

We would like to thank the following teams/people for their valuable contributions to this work. IDSU chemistry team (WuXi AppTec in Wuhan, China): Tao Guo, Duan Liu, Feng Zhao, and Pan Hu. CSU chemistry team (WuXi AppTec in Wuhan, China): Rongfeng Zhao, Shaojun Song, Wenbing Ruan. Biofizik, Inc.: Simon Bergqvist. Pfizer Boulder Research & Development: Matthew Martinson, Alex Bergstrom, Francis Sullivan. Structure Based Design, Inc.: Frank Han. WuXi Biology team (WuXi AppTec in Shanghai, China): Peipei Xu, Yingjie Li, and Chuanxiu Yang. Part of the X-ray crystallography work is based upon research conducted at the Northeastern Collaborative Access Team beamlines, which are funded by the National Institute of General Medical Sciences from the National Institutes of Health (P30 GM124165). The Eiger 16M detector on 24-ID-E is funded by a NIH-ORIP HEI grant (S10OD021527). This research used resources of the Advanced Photon Source, a U.S. Department of Energy (DOE) Office of Science User Facility operated for the DOE Office of Science by Argonne National Laboratory under Contract No. DE-AC02-06CH11357. Use of the Stanford Synchrotron Radiation Lightsource, SLAC National Accelerator Laboratory, is supported by the U.S. Department of Energy, Office of Science, Office of Basic Energy Sciences under Contract No. DE-AC02-76SF00515. The SSRL Structural Molecular Biology Program is supported by the DOE Office of Biological and Environmental Research, and by the National Institutes of Health, National Institute of General Medical Sciences (P30GM133894). The contents of this publication are solely the responsibility of the authors and do not necessarily represent the official views of NIGMS or NIH.

REFERENCES

(1) Cox, A. D.; Fesik, S. W.; Kimmelman, A. C.; Luo, J.; Der, C. J. Drugging the Undruggable RAS: Mission Possible? *Nat. Rev. Drug Discovery* **2014**, *13* (11), 828−851.

(2) Bos, J. L. Ras Oncogenes in Human Cancer: A Review. *Cancer Res.* **1989**, *49* (17), 4682−4689.

(3) Prior, I. A.; Lewis, P. D.; Mattos, C. A Comprehensive Survey of Ras Mutations in Cancer. *Cancer Res.* **2012**, *72* (10), 2457−2467.

(4) Simanshu, D. K.; Nissley, D. V.; McCormick, F. RAS Proteins and Their Regulators in Human Disease. *Cell* **2017**, *170* (1), 17−33.

(5) Fell, J. B.; Fischer, J. P.; Baer, B. R.; Blake, J. F.; Bouhana, K.; Briere, D. M.; Brown, K. D.; Burgess, L. E.; Burns, A. C.; Burkard, M. R.; Chiang, H.; Chicarelli, M. J.; Cook, A. W.; Gaudino, J. J.; Hallin, J.; Hanson, L.; Hartley, D. P.; Hicken, E. J.; Hingorani, G. P.; Hinklin,

R. J.; Mejia, M. J.; Olson, P.; Otten, J. N.; Rhodes, S. P.; Rodriguez, M. E.; Savechenkov, P.; Smith, D. J.; Sudhakar, N.; Sullivan, F. X.; Tang, T. P.; Vigers, G. P.; Wollenberg, L.; Christensen, J. G.; Marx, M. A. Identification of the Clinical Development Candidate MRTX849, a Covalent KRASG12C Inhibitor for the Treatment of Cancer. *J. Med. Chem.* **2020**, *63* (13), 6679−6693.

(6) Lanman, B. A.; Allen, J. R.; Allen, J. G.; Amegadzie, A. K.; Ashton, K. S.; Booker, S. K.; Chen, J. J.; Chen, N.; Frohn, M. J.; Goodman, G.; Kopecky, D. J.; Liu, L.; Lopez, P.; Low, J. D.; Ma, V.; Minatti, A. E.; Nguyen, T. T.; Nishimura, N.; Pickrell, A. J.; Reed, A. B.; Shin, Y.; Siegmund, A. C.; Tamayo, N. A.; Tegley, C. M.; Walton, M. C.; Wang, H.-L.; Wurz, R. P.; Xue, M.; Yang, K. C.; Achanta, P.; Bartberger, M. D.; Canon, J.; Hollis, L. S.; McCarter, J. D.; Mohr, C.; Rex, K.; Saiki, A. Y.; San Miguel, T.; Volak, L. P.; Wang, K. H.; Whittington, D. A.; Zech, S. G.; Lipford, J. R.; Cee, V. J. Discovery of a Covalent Inhibitor of KRASG12C (AMG 510) for the Treatment of Solid Tumors. *J. Med. Chem.* **2020**, *63* (1), 52−65.

(7) Chen, H.; Smaill, J. B.; Liu, T.; Ding, K.; Lu, X. Small-Molecule Inhibitors Directly Targeting KRAS as Anticancer Therapeutics. *J. Med. Chem.* **2020**, *63* (23), 14404−14424.

(8) Prior, I. A.; Hood, F. E.; Hartley, J. L. The Frequency of Ras Mutations in Cancer. *Cancer Res.* **2020**, *80* (14), 2969−2974.

(9) McGregor, L. M.; Jenkins, M. L.; Kerwin, C.; Burke, J. E.; Shokat, K. M. Expanding the Scope of Electrophiles Capable of Targeting K-Ras Oncogenes. *Biochemistry* **2017**, *56* (25), 3178−3183.

(10) Wang, H.-L.; Cee, V. J. Pyridopyrimidine Derivatives Useful as Kras G12c and Kras G12d Inhibitors in the Treatment of Cancer. WO/2021081212, April 29, 2021.

(11) Maurer, T.; Garrenton, L. S.; Oh, A.; Pitts, K.; Anderson, D. J.; Skelton, N. J.; Fauber, B. P.; Pan, B.; Malek, S.; Stokoe, D.; Ludlam, M. J. C.; Bowman, K. K.; Wu, J.; Giannetti, A. M.; Starovasnik, M. A.; Mellman, I.; Jackson, P. K.; Rudolph, J.; Wang, W.; Fang, G. Small-Molecule Ligands Bind to a Distinct Pocket in Ras and Inhibit SOS-Mediated Nucleotide Exchange Activity. *Proc. Natl. Acad. Sci. U. S. A.* **2012**, *109* (14), 5299−5304.

(12) Sun, Q.; Burke, J. P.; Phan, J.; Burns, M. C.; Olejniczak, E. T.; Waterson, A. G.; Lee, T.; Rossanese, O. W.; Fesik, S. W. Discovery of Small Molecules That Bind to K-Ras and Inhibit Sos-Mediated Activation. *Angew. Chem., Int. Ed.* **2012**, *51* (25), 6140−6143.

(13) Kessler, D.; Gmachl, M.; Mantoulidis, A.; Martin, L. J.; Zoephel, A.; Mayer, M.; Gollner, A.; Covini, D.; Fischer, S.; Gerstberger, T.; Gmaschitz, T.; Goodwin, C.; Greb, P.; Häring, D.; Hela, W.; Hoffmann, J.; Karolyi-Oezguer, J.; Knesl, P.; Kornigg, S.; Koegl, M.; Kousek, R.; Lamarre, L.; Moser, F.; Munico-Martinez, S.; Peinsipp, C.; Phan, J.; Rinnenthal, J.; Sai, J.; Salamon, C.; Scherbantin, Y.; Schipany, K.; Schnitzer, R.; Schrenk, A.; Sharps, B.; Siszler, G.; Sun, Q.; Waterson, A.; Wolkerstorfer, B.; Zeeb, M.; Pearson, M.; Fesik, S. W.; McConnell, D. B. Drugging an Undruggable Pocket on KRAS. *Proc. Natl. Acad. Sci. U. S. A.* **2019**, *116* (32), 15823−15829.

(14) Kessler, D.; Bergner, A.; Böttcher, J.; Fischer, G.; Döbel, S.; Hinkel, M.; Müllauer, B.; Weiss-Puxbaum, A.; McConnell, D. B. Drugging All RAS Isoforms with One Pocket. *Future Med. Chem.* **2020**, *12*, 1911.

(15) Sakamoto, K.; Kamada, Y.; Sameshima, T.; Yaguchi, M.; Niida, A.; Sasaki, S.; Miwa, M.; Ohkubo, S.; Sakamoto, J.; Kamaura, M.; Cho, N.; Tani, A. K-Ras(G12D)-Selective Inhibitory Peptides Generated by Random Peptide T7 Phage Display Technology. *Biochem. Biophys. Res. Commun.* **2017**, *484* (3), 605−611.

(16) Niida, A.; Sasaki, S.; Yonemori, K.; Sameshima, T.; Yaguchi, M.; Asami, T.; Sakamoto, K.; Kamaura, M. Investigation of the Structural Requirements of K-Ras(G12D) Selective Inhibitory Peptide KRpep-2d Using Alanine Scans and Cysteine Bridging. *Bioorg. Med. Chem. Lett.* **2017**, *27* (12), 2757−2761.

(17) Sogabe, S.; Kamada, Y.; Miwa, M.; Niida, A.; Sameshima, T.; Kamaura, M.; Yonemori, K.; Sasaki, S.; Sakamoto, J.; Sakamoto, K. Crystal Structure of a Human K-Ras G12D Mutant in Complex with GDP and the Cyclic Inhibitory Peptide KRpep-2d. *ACS Med. Chem. Lett.* **2017**, *8* (7), 732−736.

(18) Sakamoto, K.; Masutani, T.; Hirokawa, T. Generation of KS-58 as the First K-Ras(G12D)-Inhibitory Peptide Presenting Anti-Cancer Activity in Vivo. *Sci. Rep.* **2020**, *10* (1), 21671.

(19) Wu, X.; Upadhyaya, P.; Villalona-Calero, M. A.; Briesewitz, R.; Pei, D. Inhibition of Ras−Effector Interactions by Cyclic Peptides. *MedChemComm* **2013**, *4* (2), 378−382.

(20) Upadhyaya, P.; Qian, Z.; Selner, N. G.; Clippinger, S. R.; Wu, Z.; Briesewitz, R.; Pei, D. Inhibition of Ras Signaling by Blocking Ras−Effector Interactions with Cyclic Peptides. *Angew. Chem., Int. Ed.* **2015**, *54* (26), 7602−7606.

(21) Buyanova, M.; Cai, S.; Cooper, J.; Rhodes, C.; Salim, H.; Sahni, A.; Upadhyaya, P.; Yang, R.; Sarkar, A.; Li, N.; Wang, Q.-E.; Pei, D. Discovery of a Bicyclic Peptidyl Pan-Ras Inhibitor. *J. Med. Chem.* **2021**, *64*, 13038.

(22) Hansen, R.; Peters, U.; Babbar, A.; Chen, Y.; Feng, J.; Janes, M. R.; Li, L.-S.; Ren, P.; Liu, Y.; Zarrinkar, P. P. The Reactivity-Driven Biochemical Mechanism of Covalent KRAS G12C Inhibitors. *Nat. Struct. Mol. Biol.* **2018**, *25* (6), 454−462.

(23) Canon, J.; Rex, K.; Saiki, A. Y.; Mohr, C.; Cooke, K.; Bagal, D.; Gaida, K.; Holt, T.; Knutson, C. G.; Koppada, N.; Lanman, B. A.; Werner, J.; Rapaport, A. S.; San Miguel, T.; Ortiz, R.; Osgood, T.; Sun, J.-R.; Zhu, X.; McCarter, J. D.; Volak, L. P.; Houk, B. E.; Fakih, M. G.; O'Neil, B. H.; Price, T. J.; Falchook, G. S.; Desai, J.; Kuo, J.; Govindan, R.; Hong, D. S.; Ouyang, W.; Henary, H.; Arvedson, T.; Cee, V. J.; Lipford, J. R. The Clinical KRAS(G12C) Inhibitor AMG 510 Drives Anti-Tumour Immunity. *Nature* **2019**, *575* (7781), 217−223.

(24) Fell, J. B.; Fischer, J. P.; Baer, B. R.; Ballard, J.; Blake, J. F.; Bouhana, K.; Brandhuber, B. J.; Briere, D. M.; Burgess, L. E.; Burkard, M. R.; Chiang, H.; Chicarelli, M. J.; Davidson, K.; Gaudino, J. J.; Hallin, J.; Hanson, L.; Hee, K.; Hicken, E. J.; Hinklin, R. J.; Marx, M. A.; Mejia, M. J.; Olson, P.; Savechenkov, P.; Sudhakar, N.; Tang, T. P.; Vigers, G. P.; Zecca, H.; Christensen, J. G. Discovery of Tetrahydropyridopyrimidines as Irreversible Covalent Inhibitors of KRAS-G12C with In Vivo Activity. *ACS Med. Chem. Lett.* **2018**, *9* (12), 1230−1234.

(25) Marx, M.; Christensen, J.; Smith, C.; Fischer, J.; Burns, A. Kras G12C Inhibitors. WO/2020146613, July 16, 2020.

(26) Kawai, Y.; Shibata, K.; Asakura, H.; Uno, T.; Sagara, T.; Nakamura, M.; Kobayakawa, Y.; Holvey, R. S. A Compound Having Inhibitory Activity Against Kras G12D Mutation. WO/2021107160, June 3, 2021.

(27) Kawai, Y.; Shibata, K.; Asakura, H.; Uno, T.; Sagara, T.; Nakamura, M.; Kobayakawa, Y.; Holvey, R. S. A Compound Having Inhibitory Activity Against Kras G12D Mutation. WO/2021106231, June 3, 2021.

(28) Kurczab, R.; Śliwa, P.; Rataj, K.; Kafel, R.; Bojarski, A. J. Salt Bridge in Ligand−Protein Complexes—Systematic Theoretical and Statistical Investigations. *J. Chem. Inf. Model.* **2018**, *58* (11), 2224−2238.

(29) Degorce, S. L.; Bodnarchuk, M. S.; Cumming, I. A.; Scott, J. S. Lowering Lipophilicity by Adding Carbon: One-Carbon Bridges of Morpholines and Piperazines. *J. Med. Chem.* **2018**, *61* (19), 8934−8943.

(30) Hanessian, S.; Parthasarathy, S.; Mauduit, M.; Payza, K. The Power of Visual Imagery in Drug Design. Isopavines as a New Class of Morphinomimetics and Their Human Opioid Receptor Binding Activity. *J. Med. Chem.* **2003**, *46* (1), 34−48.

(31) Fang, Z.; Song, Y.; Zhan, P.; Zhang, Q.; Liu, X. Conformational Restriction: An Effective Tactic in 'Follow-on'-Based Drug Discovery. *Future Med. Chem.* **2014**, *6* (8), 885−901.

(32) Panigrahi, S. K.; Desiraju, G. R. Strong and Weak Hydrogen Bonds in the Protein-Ligand Interface. *Proteins: Struct., Funct., Genet.* **2007**, *67* (1), 128−141.

(33) Tóth, G.; Bowers, S. G.; Truong, A. P.; Probst, G. The Role and Significance of Unconventional Hydrogen Bonds in Small Molecule Recognition by Biological Receptors of Pharmaceutical Relevance. *Curr. Pharm. Des.* **2007**, *13* (34), 3476−3493.

https://doi.org/10.1021/acs.jmedchem.1c01688
J. Med. Chem. 2022, 65, 3123−3133

(34) Steiner, T. Unrolling the Hydrogen Bond Properties of C−H···O Interactions. *Chem. Commun.* **1997**, 727−734.
(35) Wilcken, R.; Zimmermann, M. O.; Bauer, M. R.; Rutherford, T. J.; Fersht, A. R.; Joerger, A. C.; Boeckler, F. M. Experimental and Theoretical Evaluation of the Ethynyl Moiety as a Halogen Bioisostere. *ACS Chem. Biol.* **2015**, *10* (12), 2725−2732.
(36) *Spartan'18*; Wavefunction, Inc., 2019.
(37) Keller, S.; Kneissl, J.; Grabher-Meier, V.; Heindl, S.; Hasenauer, J.; Maier, D.; Mattes, J.; Winter, P.; Luber, B. Evaluation of Epidermal Growth Factor Receptor Signaling Effects in Gastric Cancer Cell Lines by Detailed Motility-Focused Phenotypic Characterization Linked with Molecular Analysis. *BMC Cancer* **2017**, *17* (1), 845.
(38) Wang, X.; Burns, A. C.; Christensen, J. G.; Ketcham, J. M.; Lawson, J. D.; Marx, M. A.; Smith, C. R.; Allen, S.; Blake, J. F.; Chicarelli, M. J.; Dahlke, J. R.; Dai, D.; Fell, J. B.; Fischer, J. P.; Mejia, M. J.; Newhouse, B.; Nguyen, P.; O'leary, J. M.; Pajk, S.; Rodriguez, M. E.; Savechenkov, P.; Tang, T. P.; Vigers, G. P. A.; Zhao, Q. Kras G12D Inhibitors. WO/2021041571, March 4, 2021.

https://doi.org/10.1021/acs.jmedchem.1c01688
J. Med. Chem. 2022, 65, 3123−3133